

Static effective charges of BaTiO₃: Infrared spectroscopic ellipsometry study

Zhiming Huang,* Junhao Chu, Yunian Wu, Yun Hou, Jianqiang Xue, and Dingyuan Tang
*National Laboratory for Infrared Physics, Shanghai Institute of Technical Physics, Chinese Academy of Sciences,
 500 Yu Tian Road, Shanghai, 200083, People's Republic of China*

(Received 21 February 2005; published 10 August 2005)

The dielectric function of the perovskite BaTiO₃ is studied by infrared spectroscopic ellipsometry in the temperature range of 20–150 °C. A ferroelectricity-induced change of the spectral weight of the dielectric function is observed from a cubic to tetragonal structure transition. The ellipsometric data provide detailed information about the evolution of the ionic static effective charge in the cubic and ferroelectricity states. The determination of the temperature-dependent spontaneous macroscopic polarization is deduced in terms of the charge transfer of the static effective charge.

DOI: [10.1103/PhysRevB.72.052106](https://doi.org/10.1103/PhysRevB.72.052106)

PACS number(s): 78.20.Ci, 77.84.Dy, 78.20.Bh, 77.22.Ch

The mechanism of ferroelectricity is one of the main interesting problems in condensed-matter physics. It was long thought that in perovskites ABO_3 , the symmetry breaking that leads to spontaneous polarization was a collective effect, with a substantial critical polarized volume being necessary to stabilize local polarization. However, recent developments of new techniques and new materials, as well as first-principles calculations,^{1–4} have completely changed the picture of ferroelectricity.

The basic quantity in ferroelectrics is the spontaneous macroscopic polarization P , which results, e.g., upon application of an electric field, and persists at null field in two (or more) enantiomorphous metastable states of the crystal; experimentally, the difference ΔP between these states is measured by hysteresis cycles.⁵ Theoretically, the simple structures of ABO_3 allow extensive investigations. Charge-density maps and static effective charges are available based on earlier calculations for some perovskite oxides:^{6–8} although providing microscopic data relevant for the ferroelectric instability, they cannot carry quantitative information about P .⁹

Interestingly, first-principles calculations based on the dynamical atomic charges have estimated the spontaneous polarization in terms of the Born (or transverse) effective charges.^{10,11} Large values of Born effective charges were generally considered to be reliable indicators of the genuine tendency of an insulator towards ferroelectric instability. However, it may become anomalously large and independent of the amplitude of the static effective charge and two atoms with similar static effective charge also exhibit strongly different Born effective charge even in the isotropic cubic structure. Moreover, according to recent calculations, the Born effective charges do not appear to possess such a predictive capability, the inclusion of strong-correlation effects in calculations systematically reduces the magnitudes of the Born effective charges.¹²

For a long time, there has been continuing interest in the static effective charge, which lies essentially in the fact that it is an intuitive concept and helpful for a simple description of solids and molecules. It appears as a more fundamental quantity than the dynamical atomic charge since it is also one part of the dynamical atomic charge. Although several microscopic models have been postulated over the years, little

is known about any quantitative correlation between static effective charges and electronic polarization.

In this Brief Report, we propose an experimental approach to the macroscopic polarization of ferroelectrics from the static effective charges with precision optical data measurements. We performed direct ellipsometric measurements of the complex dielectric function $\epsilon(\omega) = \epsilon_1(\omega) + i\epsilon_2(\omega) = 1 + 4\pi i\sigma(\omega)/\omega$. Results are given for a paradigmatic ferroelectric: barium titanate (BaTiO₃), which is one of the most studied perovskites.

The crystal structure of BaTiO₃ has a cubic perovskite above the Curie temperature T_c , which transforms to a ferroelectric phase with a tetragonal symmetry below T_c . Two additional structural phase transitions occur at lower temperature. At 5 °C, the tetragonal phase transforms into an orthorhombic one, and then at –90 °C to a rhombohedral structure.

The samples used for spectroscopic ellipsometric measurements were melt grown BaTiO₃ crystals (see Refs. 13 and 14 for details) with multidomains in the ferroelectric phase. Spectroscopic ellipsometric measurements were carried out by an improved variable-angle infrared spectroscopic ellipsometer¹⁵ in the energy range of 4000–800 cm^{–1} at the temperature of 20–150 °C. The accuracy is better than 1% for $\tan \psi$ and $\cos \Delta$ in the measurements. The incident angle was 65° for the samples, and the difference between the ordinary and extraordinary refractive indices in our experimental energy region is less than 3%.¹⁶ Therefore the anisotropy in the ferroelectric phase is neglected.

In order to describe the dielectric function of ABO_3 in the infrared wavelength range, where the corresponding energy is higher than phonons but lower far away from band gap energy, a formula is derived to fit the above experimental data of BaTiO₃ in the following: For an electromagnetic field $E_0 e^{i\omega t}$ propagating in a material medium, a displacement x will be deduced for ions from their equilibrium positions. The equation of motion for the ions in a unit cell is

$$M^* \ddot{x} + M^* \dot{x}/\tau = qeE_0 e^{i\omega t}, \quad (1)$$

where $1/M^* = 1/M_+ + 1/M_-$ is the reduced ionic mass of cations M_+ and anions M_- in a unit cell, qe the average ionic

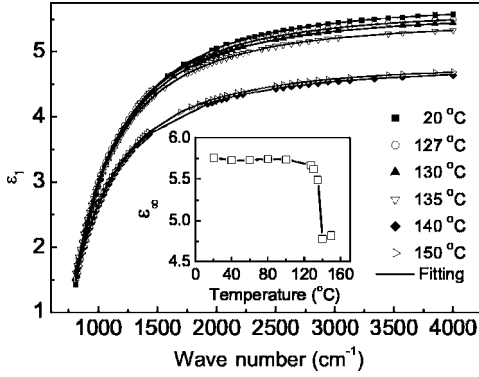


FIG. 1. Real part of the dielectric function spectra of BaTiO₃ in the infrared region and model fitting. The inset shows the variation of ϵ_∞ as a function of temperature.

static effective charges, and $qeE_0e^{i\omega t}$ the electromagnetic field force acted on atoms. τ is an energy-independent relaxation time. Restoring force, which brings ions back to the equilibrium positions, is omitted in Eq. (1). This is due to the fact that the optical frequency is high enough, and the ions response will lag. Therefore restoring force can be considered to equal zero.

The solution of Eq. (1) leads to a complex dielectric function

$$\epsilon_1(\omega) = \epsilon_\infty - \frac{4\pi e^2 q^2}{M^* \Omega} \frac{\tau^2}{1 + \omega^2 \tau^2}, \quad (2)$$

$$\sigma(\omega) = \frac{4\pi e^2 q^2}{M^* \Omega} \frac{\tau}{1 + \omega^2 \tau^2}, \quad (3)$$

where ϵ_∞ is the high frequency dielectric constant, and Ω is the unit cell volume.

Figures 1 and 2 show the complex dielectric function spectra $\epsilon_1(\omega)$ and $\sigma(\omega)$ of BaTiO₃ in the temperature range of 20–150 °C. It can be seen that the real part of the dielectric function spectra $\epsilon_1(\omega)$ and the optical conductivity spectra $\sigma(\omega)$ do not differ substantially between paraelectric and ferroelectric states in the entire energy range. In both cases, $\epsilon_1(\omega)$ exhibits a continuous increase, however, $\sigma(\omega)$ exhibits

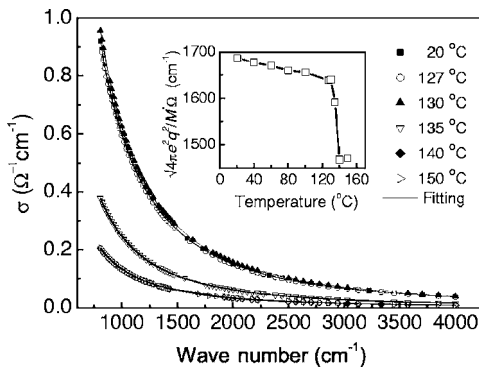


FIG. 2. Optical conductivity spectra of BaTiO₃ in the infrared region and model fitting. The inset shows the variation of $4\pi e^2 q^2 / M^* \Omega$ as a function of temperature.

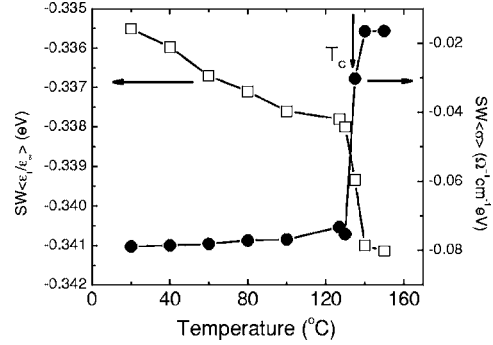


FIG. 3. Spectral weight change of (A) $\epsilon_1/\epsilon_\infty$ and (B) σ as a function of temperature through the cubic-to-tetragonal transition.

a continuous decrease toward high energy. The change of $\epsilon_1(\omega)$ in the short wavelength range is very small before 127 °C, for example, it is only about 1.5% at 4000 cm⁻¹ over a 100° temperature range. Then it decreases faster and faster when the temperature increases to 135 °C. The change is $\sim 1.0\%$ at 4000 cm⁻¹ from 127 to 130 °C, it is $\sim 2.0\%$ from 130 to 135 °C. When the temperature reaches from 135 to 140 °C, $\epsilon_1(\omega)$ drops dramatically, the change reaches $\sim 12.7\%$. On the other hand, $\sigma(\omega)$ displays contrary rules. The change of $\sigma(\omega)$ in the long wavelength range is small before 130 °C. Then it increases when the temperature increases. The fitted dielectric function spectra by Eqs. (2) and (3) are also shown in Figs. 1 and 2, respectively. Excellent agreements are found between model fitting and experimental data in the energy range of 4000–800 cm⁻¹.

Ellipsometry has the advantage that it measures the complex dielectric function directly without the usage of the Kramers-Kronig(KK) relation. Its self-normalizing nature allows us to analyze the temperature-distribution of the spectral weight (SW) of $\sigma(\omega)$ and $\epsilon_1(\omega)$ in the cubic and ferroelectric states for ferroelectrics. As shown in the insets of Figs. 1 and 2, ϵ_∞ and $4\pi e^2 q^2 / M^* \Omega$ are the function of temperature, the finite sum rule of $SW\langle\sigma\rangle = \int_{\omega_1}^{\omega_2} \sigma(\omega) d\omega$ has been calculated for $\sigma(\omega)$ and $SW\langle\epsilon_1/\epsilon_\infty\rangle = \int_{\omega_1}^{\omega_2} \epsilon_1(\omega) / \epsilon_\infty d\omega$ for $\epsilon_1(\omega) / \epsilon_\infty$. Figure 3 shows the integration results of $SW\langle\sigma\rangle$ and $SW\langle\epsilon_1/\epsilon_\infty\rangle$ with the upper integration limit $\omega_2 = 4000$ cm⁻¹ and lower integration limit $\omega_1 = 800$ cm⁻¹ as a function of temperature. There is an abrupt decrease for the spectral weight $SW\langle\sigma\rangle$ near the paraelectric-to-ferroelectric transition temperature (T_c), which reveals that an anomalous ferroelectricity-induced $SW\langle\sigma\rangle$ decreases in the energy range of 4000–800 cm⁻¹. The temperature dependence of $\epsilon_1(\omega)$ affords an independent and complementary way to analyze the $SW\langle\sigma\rangle$ variation. The decrease of $SW\langle\sigma\rangle$ gives rise to an increase of $\epsilon_1(\omega)$ from the paraelectric-to-ferroelectric transition. It should be emphasized that this is a model-independent conclusion based solely on the KK relation between $\epsilon_1(\omega)$ and $\sigma(\omega)$, both of which are directly measured by ellipsometry.

The related SW changes can be quantified using the static effective charge, which can be derived from the inset of Fig. 2. The lattice parameters in the calculations were taken from Refs. 17 and 18. The temperature dependence evolution of

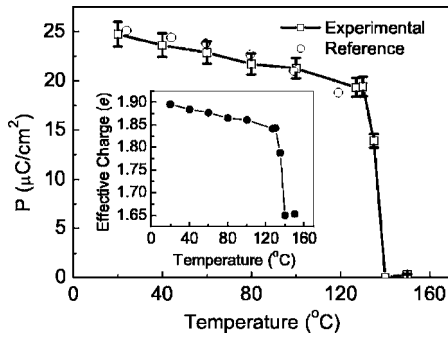


FIG. 4. The spontaneous polarization of BaTiO_3 vs temperature. The open circles are taken from experimental data (Ref. 13). The closed circles are calculated in terms of the static effective charges. The inset shows the temperature-dependent evolution of the static effective charge.

the static effective charge is displayed in the inset of Fig. 4. The static effective charge appears to be composed of two terms for BaTiO_3 in the ferroelectric phase. The first one is the hopping contribution through cubic-to-tetragonal structure transition: it leads to the modification of the interatomic distance, which is characterized by a small uniaxial macroscopic strain, accompanied by microscopic displacements of the ions out of their high-symmetry sites: the latter distortion determines a preferred polarity of the tetragonal axis, and is responsible, upon symmetry grounds, for the occurrence of P . The second is the temperature-dependent charge component: it originates in the effect of charge transfer in unit cells and relates to the cell volume as temperature. It contributes to the macroscopic polarization only in the ferroelectric phase when the ions are out of the high-symmetry sites. We obtain $|q| = 1.65 \pm 0.0066$ and 1.90 ± 0.0058 , respectively, for 140 and 20 °C from the inset of Fig. 4. In particular for anions, the average effective charge of oxygen atoms is -1.65 ± 0.0066 at 140 °C and -1.90 ± 0.0058 at 20 °C, respectively. The effective charge of -1.65 in the cubic phase is remarkably close to that of -1.63 from first-principles calculations,⁸ which supports the correctness of our model.

Different approaches have been considered in order to evaluate the amplitude of the static effective charges for BaTiO_3 .^{19–23} All the calculations reveal that the charge transfer from Ti to O is not complete. If BaTiO_3 were a purely ionic crystal, the $3d$ and $4s$ electrons of Ti would be entirely transferred to the oxygen atoms, yielding a charge of -2 on oxygen. However, due to the partial hybridization between O $2p$ and Ti $3d$ states,^{6,8,24} these electrons remain partly delocalized on the Ti atoms so that the static charges on the Ti and O atoms are smaller than they would be in a purely ionic material. The charge transfer from the Ti to O atoms favors the static effective charge in the ferroelectric phases.

Based on the static effective charge concept, the spontaneous polarization is defined by the net value of the charge transfer in one unit cell, relative to the static effective charge of the paraelectric cubic phase, per unit area on the surface perpendicular to the axis of spontaneous polarization

$$P = \Delta Q/A_0 = (Q - Q_0)/A_0, \quad (4)$$

where Q_0 and Q are the experimental ionic static effective charges in cubic and ferroelectric structures for ABO_3 , respectively, and A_0 is the area perpendicular to the axis of spontaneous polarization.

The spontaneous polarization of BaTiO_3 versus temperature is calculated by Eq. (4) and shown in Fig. 4. A remarkable agreement is obtained between the experimental and reference data (Ref. 13) below T_c . We emphasize that our model is based on the static effective charge in one unit cell and no detailed information is required for the displacement of the centers of gravity of the negative and positive charges within the unit cell, which was thought to be stabilized by long-range Coulomb interactions. Therefore our results indicate that the spontaneous polarization originates from the charge transfer related to the cubic phase, in which no substantial critical polarized volume is necessary to stabilize local polarization.

To further testify it, we expect the possible maximal values of the spontaneous polarization for the additional two ferroelectric structures using the static effective charges and compare with experiments, based on the fact that the maximum possible amount of the static effective charge is $\Delta Q \approx 0.35e$ without strain²⁵ ($|q| = 2.0$ is assumed for a complete charge transfer that occurred in orthorhombic and rhombohedral phases). All the structural information is obtained from Refs. 17 and 26. In terms of Eq. (4), the calculated P is 24.4 ± 1.2 , $19.9 \pm 1.0 \mu\text{C}/\text{cm}^2$ for orthorhombic and rhombohedral phases, compared with the maximal experimental values of 26.8 and $19.3 \mu\text{C}/\text{cm}^2$, respectively.²⁷ The quantitative agreements also support the fact that the spontaneous polarization is facilitated by charge transfer of the static effective charge. The maximum degree of charge transfer can be as high as $\sim 21\%$ without strain, relative to that in the cubic phase.

In conclusion, our spectroscopic ellipsometric measurements on BaTiO_3 suggest a ferroelectricity-induced SW change of the dielectric function and have demonstrated the static effective charge approach to determine the polarization of BaTiO_3 . The spontaneous macroscopic polarization for BaTiO_3 is predicated well both as a function of temperature in tetragonal structure and in additional two ferroelectric phases in one unit cell, which suggests that the spontaneous polarization is driven by the static effective charge transfer and no substantial critical polarized volume is necessary to stabilize local polarization. It is anticipated that this work will stimulate theoretical investigations on the static effective charges for predicting the spontaneous macroscopic polarization and pyroelectricity of solids and to understand the mechanisms of ferroelectricity at the nanoscale.

The authors are grateful to Z. G. Hu, H. S. Luo, D. Q. Liu, W. L. Xu, X. J. Meng, and G. S. Wang for useful discussions. This work was supported by National Grant Foundation Project (No. G001CB3095), National Natural Science Foundation (No. 60407014 and 60221502), and Shanghai Grants (No. 02DJ14001).

*Electronic address: zmhuang@sh163.net

- ¹C. H. Ahn, K. M. Rabe, and J.-M. Triscone, *Science* **303**, 488 (2004).
- ²T. Tybell, C. H. Ahn, and J.-M. Triscone, *Appl. Phys. Lett.* **75**, 856 (1999).
- ³M. Dawber, P. Chandra, P. B. Littlewood, and J. F. Scott, *J. Phys.: Condens. Matter* **15**, L393 (2003).
- ⁴R. Yu and H. Krakauer, *Phys. Rev. Lett.* **74**, 4067 (1995).
- ⁵M. E. Lines and A. M. Glass, *Principles and Applications of Ferroelectrics and Related Materials* (Clarendon, Oxford, 1977).
- ⁶R. H. Cohen, *Nature (London)* **358**, 136 (1992); R. H. Cohen and H. Krakauer, *Ferroelectrics* **136**, 65 (1992).
- ⁷Y.-N. Xu, W. Y. Ching, and R. H. French, *Ferroelectrics* **111**, 23 (1990); Y.-N. Xu, Hong Jiang, Xue-Fu Zhong, and W. Y. Ching, *ibid.* **153**, 19 (1994).
- ⁸R. E. Cohen and H. Krakauer, *Phys. Rev. B* **42**, 6416 (1990).
- ⁹R. M. Martin, *Phys. Rev. B* **9**, 1998 (1974).
- ¹⁰R. Resta, M. Posternak, and A. Baldereschi, *Phys. Rev. Lett.* **70**, 1010 (1993); H. J. Bakker, S. Hunsche, and H. Kurz, *Phys. Rev. B* **48**, 9331 (1993).
- ¹¹W. Zhong, R. D. King-Smith, and D. Vanderbilt, *Phys. Rev. Lett.* **72**, 3618 (1994).
- ¹²A. Filippetti and N. A. Spaldin, *Phys. Rev. B* **68**, 045111 (2003).
- ¹³S. H. Wemple, M. DiDomenico, Jr., and I. Camlibel, *J. Phys. Chem. Solids* **29**, 1797 (1968).
- ¹⁴J. L. Servoin, F. Gervais, A. M. Quittet, and Y. Luspin, *Phys. Rev. B* **21**, 2038 (1980).
- ¹⁵Z. M. Huang and J. H. Chu, *Appl. Opt.* **39**, 6390 (2000).
- ¹⁶E. D. Palik, *Handbook of Optical Constants of Solids II* (Academic, San Diego, 1991).
- ¹⁷Y. H. Xu, *Ferroelectric Materials and Their Applications* (Elsevier, Amsterdam, 1991).
- ¹⁸Ph. Ghosez, X. Gonze, and J.-P. Michenaud, *Ferroelectrics* **206**, 205 (1998).
- ¹⁹W. A. Harrison, *Electronic Structure and the Properties of Solids* (Freeman, San Francisco, 1980).
- ²⁰A. W. Hewat, *J. Phys. C* **6**, 1074 (1973).
- ²¹D. Khatib, R. Migoni, G. E. Kugel, and L. Godefroy, *J. Phys.: Condens. Matter* **1**, 9811 (1989).
- ²²A. V. Turik and A. G. Khasabov, *Ferroelectrics* **83**, 165 (1988); **164**, 345 (1995).
- ²³F. M. Michel-Calendini, H. Chermette, and J. Weber, *J. Phys. C* **13**, 1427 (1980).
- ²⁴L. T. Hudson, R. L. Kurtz, S. W. Robey, D. Temple, and R. L. Stockbauer, *Phys. Rev. B* **47**, 1174 (1993).
- ²⁵N. Yanase, K. Abe, N. Fukushima, and T. Kawakubo, *Jpn. J. Appl. Phys., Part 1* **38**, 5305 (1999).
- ²⁶T. Mitsui *et al.*, *Oxides, Landolt-Bornstein Numerical Data and Functional Relationships in Science and Technology, Group III, Vol. 16, Pt. a* (Springer-Verlag, Berlin, 1981).
- ²⁷H. H. Wieder, *Phys. Rev.* **99**, 1161 (1955).